Chemical Science

ROYAL SOCIETY OF CHEMISTRY

EDGE ARTICLE

View Article Online
View Journal | View Issue

Cite this: *Chem. Sci.*, 2024, **15**, 18933

All publication charges for this article have been paid for by the Royal Society of Chemistry

A hot exciton organic glassy scintillator for high-resolution X-ray imaging†

Xi Yang,[ab] Jingru Chen,[c] Yang Zhang,[c] Yiming Di,[c] Guozhen Zhang,[c] Songhua Chen, *[b] Hongming Chen*[a] and Mei-Jin Lin *[ac]

Received 19th August 2024
Accepted 17th October 2024

DOI: 10.1039/d4sc05544f

rsc.li/chemical-science

Hot exciton organic scintillators offer promising prospects due to their efficient generation of bright triplet excitons and ultrafast response time, having potential applications in security detection and medical diagnostics. However, fabricating large-area, highly transparent scintillator screens still remains challenging, impeding the realization of high-resolution X-ray imaging. Herein, we firstly demonstrate a novel highly-transparent hot exciton organic glassy scintillator (>87% transmittance @ 450–800 nm), produced using a low-temperature melt-quenching method with 2′,5′-difluoro-*N*4,*N*4,*N*4″,*N*4″-tetraphenyl-[1,1′:4′,1″-terphenyl]-4,4″-diamine (DTPA2F) powder. Remarkably, compared to crystalline DTPA2F, which has a photoluminescence quantum yield of 67.8% and a relative light yield of 46 400 ± 406 photons MeV^{-1}, the DTPA2F glass retains 49.8% and 28 341 ± 246 photons MeV^{-1}, respectively. This results in a low detection limit of about 53.7 nGy s^{-1} and an ultrafast decay time of 1.66 ns for DTPA2F glass. Besides, it exhibits excellent environmental stability with no recrystallization or degradation after over 100 days of exposure to ambient conditions. Furthermore, the scintillator screen demonstrates exceptional spatial resolution of 38.5 lp mm^{-1} for X-ray imaging. It provides a simple molecular design strategy and a screen fabrication method for developing large-area, highly-transparent, efficient and ultrafast organic glassy scintillators.

Introduction

Scintillators have attracted considerable attention owing to their important applications in security detection, medical imaging and non-destructive inspection.[1] Presently, inorganic scintillators $Bi_4Ge_3O_{12}$ (BGO) and CsI:Tl single crystals are widely applied in industrial and medical fields due to their excellent comprehensive radioluminescence properties. However, the growth of transparent, large-sized inorganic single crystal scintillators typically requires the use of the Czochralski method, which involves high growth temperatures and extended time periods.[2] It presents a huge challenge in achieving large-area, high-performance scintillators through economical and easily reproducible methods. In recent years, there has been growing interest in organic thermally activated delayed fluorescence (TADF) and room-temperature phosphorescence (RTP) scintillators due to their potential to achieve efficient scintillators with a theoretical exciton utilization efficiency of 100%.[3–5] Despite significant progress, balancing high scintillation efficiency with fast timing properties in these materials remains challenging. They typically exhibit scintillation lifetimes ranging from microseconds to even seconds through the phosphorescence or delayed fluorescence emission process, potentially limiting their suitability for fast response X-ray detection and imaging.

In contrast to TADF and RTP molecules, organic "hot exciton" materials hold promise in overcoming the challenge of balancing high scintillation efficiency and fast timing properties, achieving efficient and rapid X-ray luminescence. This is because they can achieve hybridized local and charge-transfer (HLCT) emission through high-level reverse intersystem crossing (H-RISC) from high-lying triplet states (T_n; $n \geq 2$) to singlet states (S_m; $m \geq 1$) (Scheme 1a).[6,7] This emission process can effectively utilize triplet excitons, significantly enhancing radioluminescence (RL) intensity while ensuring nanosecond-scale decay lifetimes, thus greatly reducing the impact of afterglow during X-ray imaging. Recently, Yang *et al.* first reported a novel hot exciton organic scintillator, the 1,8-naphthalimide-phenothiazine (OMNI-PTZ2) compound, which showed a low X-ray detection limited (97 nGy s^{-1}) and a fast decay time (13.8 ns) in its crystalline powder due to its effective utilization of triplet excitons through the H-RISC process.[8] After that, Tang *et al.* reported the hot exciton organic scintillator

[a]*College of Materials Science and Engineering, Fuzhou University, Fuzhou, 350116, P.R. China. E-mail: chm@fzu.edu.cn; meijin_lin@fzu.edu.cn*

[b]*College of Chemistry and Material, Longyan University, Longyan, 364000, P. R. China. E-mail: songhua@iccas.ac.cn*

[c]*College of Chemistry, Fuzhou University, Fuzhou, 350116, P.R. China*

† Electronic supplementary information (ESI) available: Experimental procedures, characterization, and additional spectra and other relevant data. CCDC 2357920 and 2357922. For ESI and crystallographic data in CIF or other electronic format see DOI: https://doi.org/10.1039/d4sc05544f

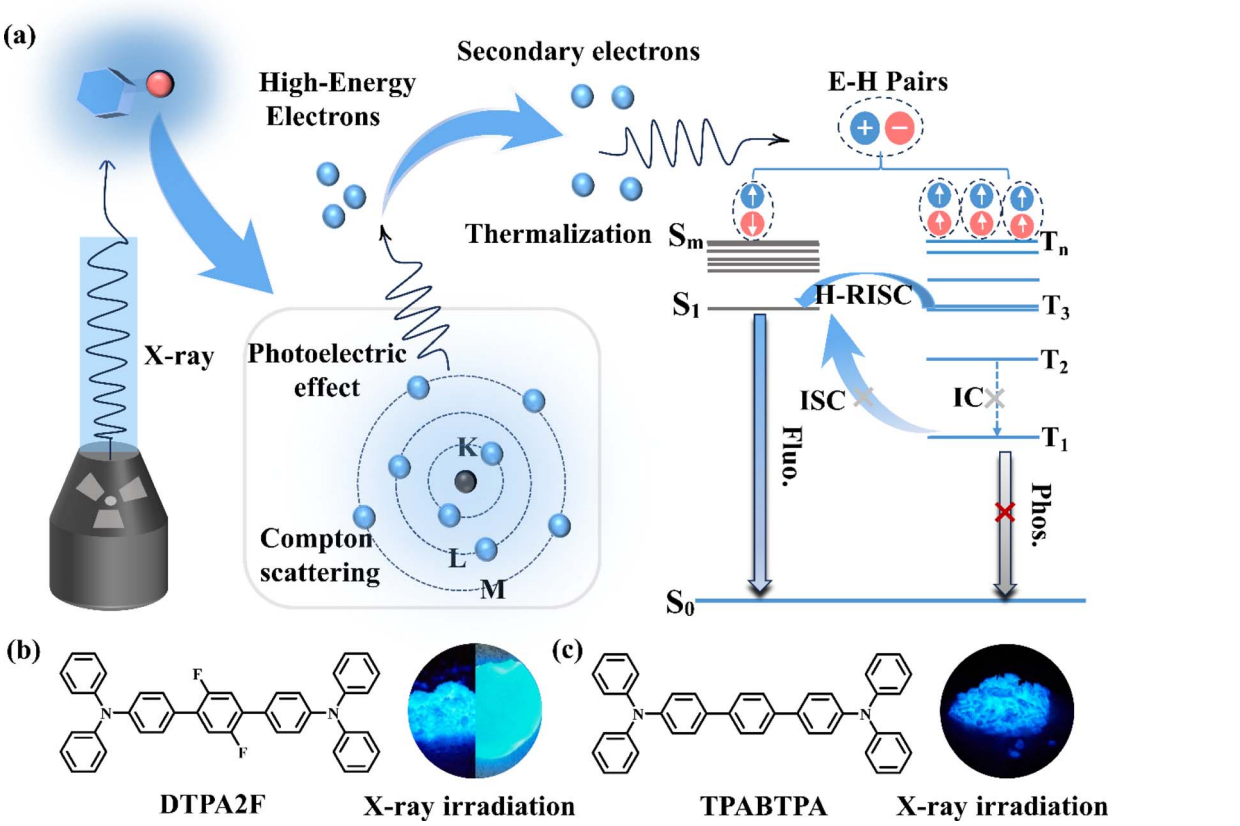

Scheme 1 (a) Schematic diagram of the X-ray-excited luminescence process in hot exciton scintillators. Molecular structures and X-ray-excited luminescence images of (b) the hot exciton dye DTPA2F (powder and glass) and (c) the fluorescence dye TPABTPA.

TPE-4Br, with a light yield of up to 34 600 photons MeV^{-1} and a decay time as low as 1.79 ns for its single crystal,[9] making TPE-4Br a superior alternative to conventional scintillators (such as anthracene) and some inorganic scintillators.[10] However, when utilizing these materials for X-ray imaging applications, both of them doped organic molecules into a polymeric matrix to prepare scintillator screens. This leads to a notable decrease in scintillation performance and renders the screens opaque, causing light scattering during X-ray imaging, thereby impeding the achievement of ultra-high spatial resolution with low X-ray doses.[11]

Glass-state scintillation materials, as a type of transparent material that can be mass-produced with uniform composition, can significantly reduce the light scattering effect caused by the dispersion of scintillator microcrystals in a polymer matrix, thereby improving the light output efficiency of scintillator materials and achieving high-resolution X-ray imaging.[12,13] In recent years, some metal halide luminescent materials that can be prepared as glass-state materials were employed as scintillators and showed good performance in X-ray detection.[14,15] However, when these ionic metal halides transition from crystalline to glass-state materials, significant radioluminescence quenching typically occurs due to the destruction of the crystal structure.[16,17] Additionally, the ionic migration properties of these scintillators make them susceptible to environmental interference, causing them to recrystallize or decompose easily, which limits their practical application. Moreover, these materials typically have long decay lifetimes, which are detrimental to eliminating the afterglow in X-ray imaging.[18] Recently, we designed and synthesized organic scintillator glasses based on maleimide derivatives, which feature easy large-area preparation, high optical transparency, and short decay time, achieving excellent X-ray imaging (>20.0 lp mm^{-1}). However, these fluorescent dyes only utilize 25% of singlet excitons for luminescence, resulting in relatively weak RL intensity.[19] Therefore, the development of hot exciton organic dyes that can be processed into glass-state materials will lead to organic scintillators with high exciton utilization efficiency, rapid scintillation, high transparency, and low-cost large-scale production potential, making them highly promising for high-resolution X-ray imaging.

To prove this concept, we synthesized *N*4,*N*4,*N*4″,*N*4″-tetraphenyl-[1,1′:4′,1″-terphenyl]-4,4″-diamine (TPABTPA) and 2′,5′-difluoro-*N*4,*N*4,*N*4″,*N*4″-tetraphenyl-[1,1′:4′,1″-terphenyl]-4,4″-diamine (DTPA2F) molecules, achieving the transition from conventional fluorescent TPABTPA to hot exciton dye DTPA2F by modulating F atom substitution. Compared to the TPABTPA molecule, the DTPA2F molecule can effectively utilize triplet excitons through the H-RISC process to achieve HLCT emission. This results in the observation that, although DTPA2F and TPABTPA crystalline powders have similar PLQYs ($\Phi_{f,DTPA2F}$ = 67.8%, $\Phi_{f,TPABTPA}$ = 63.3%), the former exhibits twice the RL

intensity of the latter with a relative light yield as high as 46 400 ± 406 photons MeV^{-1}. Besides, DTPA2F crystalline powder can be converted into a glass-state *via* a simple low-temperature melt-quenching method. The PLQY and relative light yield of DTPA2F glass can reach 49.8% and 28 341 ± 246 photons MeV^{-1}, respectively. It makes DTPA2F glass showed a high RL intensity (approximately 114% of BGO), a low detection limit of 53.7 nGy s^{-1}, and an ultrafast decay time of 1.66 ns. More importantly, it exhibits an excellent environmental stability, showing no recrystallization or degradation after over 100 days of exposure to ambient conditions (25 °C, 60% relative humidity). Furthermore, with >87% transmittance in the range of 450–800 nm, the DTPA2F scintillator screen minimizes afterglow and light scattering interference during X-ray imaging, thus demonstrating outstanding performance. It exhibits exceptional spatial resolution of 38.5 lp mm^{-1} for X-ray imaging, allowing clear visualization of small fish skeletons and copper mesh. It introduces the concept of hot exciton organic glassy scintillators for the first time, offering a new pathway for developing efficient and fast scintillators with high transparency, easy large-area, and low-cost preparation.

Results and discussion

As shown in Scheme 1b, c and Fig. S1, S2,† the two structurally similar molecules, DTPA2F and TPABTPA, were synthesized using a Pd-catalyzed Suzuki coupling reaction.[6] Their chemical and crystal structures were confirmed using ^{1}H NMR, ^{13}C NMR, and single-crystal X-ray diffraction (XRD) (Fig. S3–S6†). Based on the crystal structures of DTPA2F and TPABTPA, we initially employed time-dependent density functional theory (TD-DFT) to calculate and analyze the ground-state electron cloud distribution and excited-state energy levels of these molecules. As shown in Fig. 1a and b, both DTPA2F and TPABTPA molecules exhibit similar electronic distributions. Their lowest unoccupied molecular orbitals (LUMO) are mainly localized on the three central benzene rings, while the highest occupied molecular orbitals (HOMO) are distributed throughout the molecular skeleton. This orbital overlap between the HOMO and LUMO can effectively enhance their fluorescence efficiency.[20] Besides, the analysis of their excited-state energy levels revealed that DTPA2F possesses typical energy level characteristics of hot exciton materials. As can be seen in Fig. 1a, the energy gap between S_1 and S_0 is as high as 1.7915 eV, whereas the energy gap between S_1 and the higher triplet state T_3 is less than 0.03 eV (0.0284 eV). And the spin–orbit coupling strength (SOC, ξ) between S_1 and T_3 is 0.709 cm^{-1}, significantly exceeding ξ (S_1, T_1) at 0.081 cm^{-1} (Table S1†). This disparity leads to the RISC rate from higher triplet state T_3 to S_1 being much higher than the RISC rate from T_1 to S_1. Consequently, it facilitates the RISC process for excitons from T_3 to S_1 more readily than from T_1 to S_1.[21] Additionally, the energy gaps between T_3 and T_2, as well as between T_2 and T_1, are as high as 0.61 eV and 0.75 eV, which effectively suppresses the internal conversion process from T_3 to T_2 and from T_2 to T_1.[22] As a result, the DTPA2F molecule can effectively utilize triplet excitons by the H-RISC process, resulting in HLCT emission.[23,24] In contrast, although the ξ (S_1, T_3) of the TPABTPA molecule (0.790 cm^{-1}) is significantly higher than ξ (S_1, T_1) at 0.156 cm^{-1}, its energy gaps from T_3 to T_2 and from T_2 to T_1 are only 0.23 and 0.32 eV, respectively (Table S1†). This indicates that triplet excitons can easily convert to the T_1 level through internal conversion,[25] which do not meet the requirement for undergoing the H-RISC process from the high triplet states T_n to the singlet state S_1. Therefore, the TPABTPA molecule is considered to be a fluorescent dye.[23]

Combining the emission and absorption spectral changes of the DTPA2F and TPABTPA molecules in different polar solvents further experimentally confirms the accuracy of the above theoretical analysis. As shown in Fig. 1d–f, the red shifts in the fluorescence emission spectra of DTPA2F and TPABTPA from low-polarity solvents to high-polarity solvents are 45 and 59 nm, respectively.[26] Using the Lippert–Mataga model based on the Stokes shift and solvent orientation polarizability (Fig. S7 and Tables S2, S3†), it was found that the fit line of the Stokes shift *versus* solvent polarity (*f*) for DTPA2F displays two different slopes.[27,28] This indicates the presence of two distinct excited states: a locally excited (LE) state in low-polarity solvents and a charge transfer (CT) state in high-polarity solvents (Fig. 1d).[28] In contrast, the fit line for TPABTPA shows only one slope, indicating that TPABTPA is a conventional fluorescent molecule. Thus, we have theoretically and experimentally demonstrated that DTPA2F exhibits emission characteristics of HLCT states, making it an organic hot exciton molecule.

In addition, the excitation peaks of DTPA2F and TPABTPA powders are located at 418 nm, with emission peaks at 443 and 447 nm, respectively (Fig. 1f). Compared to TPABTPA, DTPA2F exhibits a smaller Stokes shift, indicating that it can convert excitation energy into photons more efficiently.[29] Both DTPA2F and TPABTPA powders show rapid single-exponential decay times of 1.52 and 2.13 ns (Fig. 1d), meaning that their luminescence afterglow can be negligible in X-ray imaging applications.[30] Furthermore, the PLQYs of DTPA2F and TPABTPA crystalline powders are 67.8% and 63.3% (Fig. 1h and S8a, b†). Given that their solid-state photoluminescence properties are strongly related to their crystal structures,[31] we conducted a detailed investigation. As shown in Fig. S9 and Table S4,† DTPA2F and TPABTPA have similar molecular packing, and they both belong to the triclinic $P\bar{1}$ space group. However, the introduction of F atoms in DTPA2F increases the twist angles between adjacent phenyl rings. Specifically, the twist angle between the *p*-phenylene and adjacent benzene rings in the DTPA2F molecule is 48.12°, while the angle between the diphenylamine unit and adjacent benzene rings is 69.33°. These angles are significantly larger than those in TPABTPA, being 20.44° and 61.19°, respectively.[32] This twisted structure in the DTPA2F molecule effectively reduces aggregation-induced quenching, thereby enhancing its luminescent properties.[33]

The introduction of F atoms can further enrich the intermolecular interactions in DTPA2F molecules. As shown in Fig. S10a and b,† the two-dimensional fingerprint plots of these crystals, analyzed using Hirshfeld surfaces with CrystalExplorer software,[32] revealed the relative contributions of various weak intermolecular interactions. Compared to TPABTPA, which

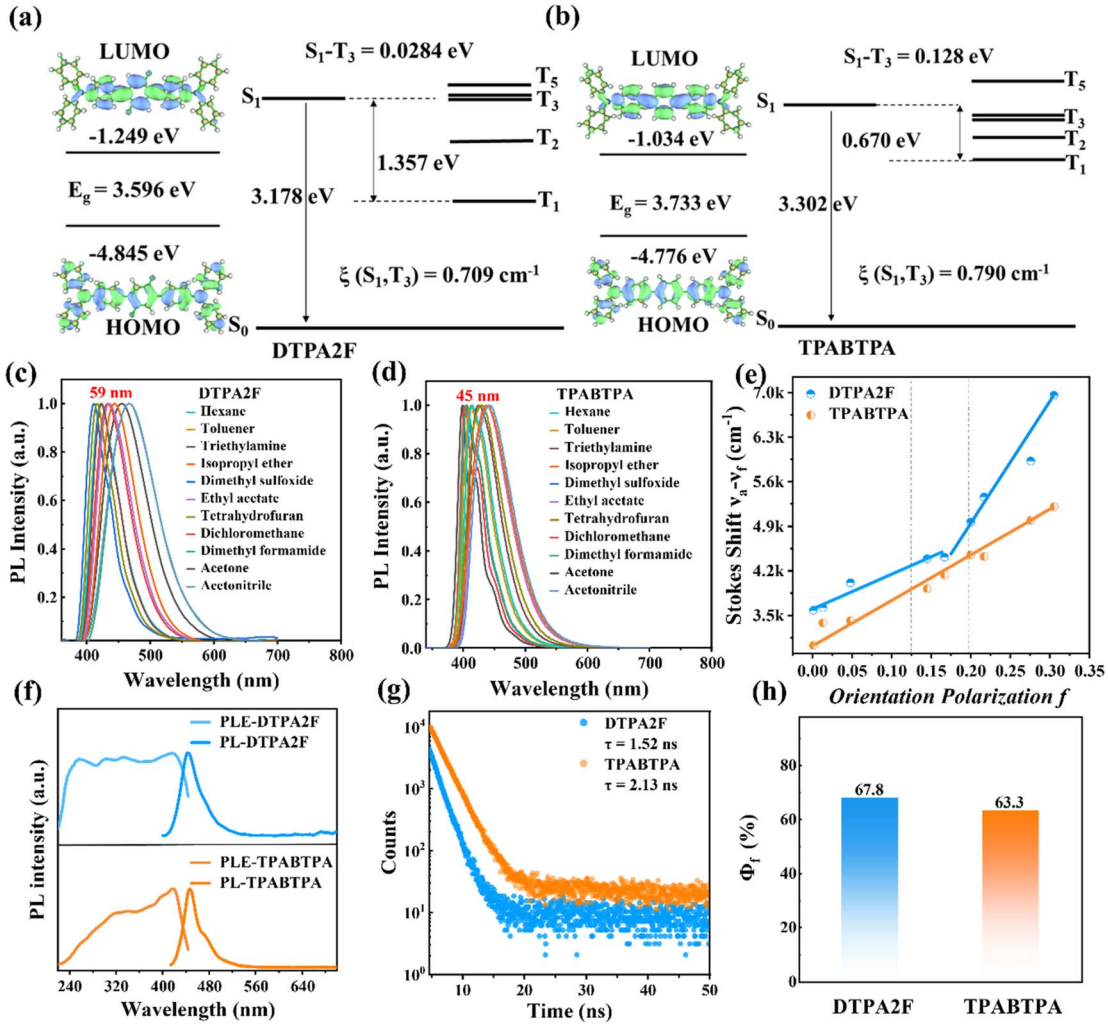

Fig. 1 Photophysical properties of DTPA2F and TPABTPA. The HOMO/LUMO distributions and energy level diagrams of the singlet and triplet excited states of (a) the DTPA2F molecule and (b) the TPABTPA molecule. Normalized photoluminescence (PL) spectra in various solvents (1×10^{-5} mol L^{-1}) of (c) DTPA2F and (d) TPABTPA. (e) Lippert–Mataga plots of DTPA2F and TPABTPA molecules. (f) Excitation and emission spectra. (g) Time-resolved PL decay spectra and (h) the PLQYs of DTPA2F and TPABTPA crystalline powders.

primarily shows strong contributions from H···H interactions (64.3%) and C···H interactions (33.8%), DTPA2F exhibits a more diverse range of intermolecular interactions, including H···H (52.7%), C···H (33.5%), C···F (0.3%), and H···F (11.8%). These interactions restrict the free rotation of the phenyl groups and lead to a denser molecular packing model of the DTPA2F crystal. The more twisted structure and richer intermolecular interactions of a DTPA2F single crystal effectively limit the free rotation of the benzene ring, block non-radiative pathways and prevent fluorescence quenching, thereby ensuring a higher PLQY for DTPA2F powder.[33]

Given the good photoluminescence properties of DTPA2F and TPABTPA crystalline powders, we further measured their RL spectra under an X-ray dose rate of 278 μGy s^{-1}. As shown in Scheme 1b, c and Fig. 2a, both materials exhibited bright blue luminescence under X-ray irradiation, with emission peaks at 464 nm for DTPA2F and 469 nm for TPABTPA. The RL intensity of DTPA2F powder reached 4.63×10^5 a.u., which is twice that of TPABTPA powder (2.30×10^5 a.u.) and 1.49 times that of the BGO single crystal (3.11×10^5 a.u.). Considering their nearly identical X-ray absorption coefficients (Fig. S11†)[36] and similar PLQYs, the significantly enhanced RL intensity of DTPA2F powder primarily arises from its higher exciton utilization efficiency.[37] DTPA2F can theoretically achieve 100% exciton utilization through the H-RISC process (Scheme 1a), while TPABTPA can only utilize 25% of singlet excitons.

This further demonstrates that organic hot exciton dyes are highly promising for the development of superior organic scintillators. Besides, based on eqn (S1)–(S3) and Fig. S12,† the relative light yield of DTPA2F is estimated to be 46 405 ± 406 photons MeV^{-1} by using BGO as a reference (8000 photons MeV^{-1}).[38] Notably, the calculated light output of DTPA2F is higher than that of most typical scintillators (Fig. 2b). Its ultrafast single exponential decay time of 1.52 ns is obviously better than that of other organic scintillator materials (Fig. 2b). DTPA2F provides significant advantages for high-performance

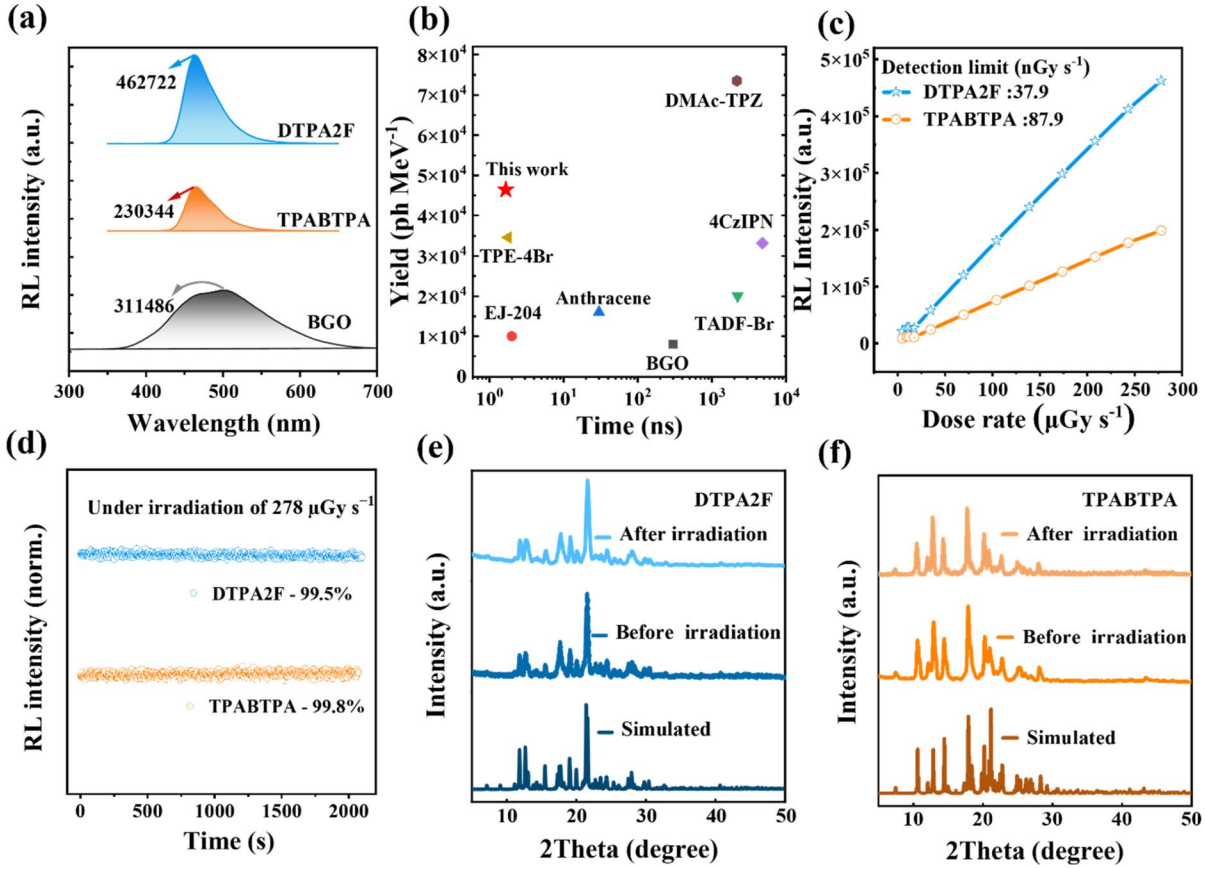

Fig. 2 Scintillation properties of DTPA2F and TPABTPA crystalline powders. (a) The RL spectra of DTPA2F, TPABTPA and BGO at the X-ray dose of 278 μGy s^{-1} and (b) their corresponding relative light yield *versus* decay time with some reported scintillators.[9,34,35] (c) Their maximum RL intensity *versus* X-ray dose rates from 4.58 to 278 μGy s^{-1}. (d) Their emission stability under continuous X-ray irradiation (278 μGy s^{-1}, 2000 s). The powder XRD before and after X-ray irradiation for (e) DTPA2F and (f) TPABTPA powders.

detection systems by effectively balancing ultra-fast decay time and high scintillation performance.[34,39] Additionally, the RL spectra of DTPA2F and TPABTPA powders were collected at various X-ray dose rates (Fig. S13a and S13b†) to assess their detection limits (LOD).[36] As shown in Fig. 2c, the RL intensities of both materials increased with rising X-ray dose rates from 4.58 to 278 μGy s^{-1} and exhibited commendable linearity in response to X-ray dose rates. Using a signal-to-noise ratio of 3,[36] the calculated detection limits for DTPA2F and TPABTPA were about 37.9 and 87.9 nGy s^{-1}, respectively. Both of them are significantly lower than the standard dose rate for medical X-ray diagnostics (5.50 μGy s^{-1}), with the LOD of DTPA2F being just 1/145th of this standard.[40] Moreover, the RL intensities of DTPA2F and TPABTPA crystalline powders maintain over 99% of their initial values after continuous irradiation for 2000 s at the X-ray dose rate of 278 μGy s^{-1} (Fig. 2d). And their powder XRD analysis showed negligible change before and after X-ray irradiation (Fig. 2e and f), indicating that the structural integrity of the materials remained unchanged under X-ray exposure, further evidencing their good irradiation stability.[41]

Considering the excellent scintillation properties of DTPA2F, we aim to prepare it into a scintillator screen for X-ray imaging. Currently, researchers primarily achieve X-ray imaging by growing organic scintillator single crystals of a certain size (>1 cm^2)[2] or by doping scintillator microcrystals (5–60 wt%) into a polymer matrix to create scintillator thin films.[5,42] The former requires a lengthy single crystal growth process (ranging from several days to several weeks) and is typically difficult to control in terms of thickness and size, severely limiting its application.[43] The latter method, although capable of producing large-area films, significantly reduces the content of organic scintillators, thereby impairing their RL intensity. Additionally, high doping levels often result in opaque films, leading to optical scattering during imaging, which severely degrades image quality.[11]

Therefore, we focused on studying the thermodynamic properties of the two molecules to explore the feasibility of fabricating them into glassy films. As shown in Fig. S14,† thermogravimetric analysis (TGA) indicated that the decomposition temperature (T_d) of DTPA2F is 411 °C, demonstrating good thermal stability. In addition, differential scanning calorimetry (DSC) measurements revealed that the melting temperature (T_m) of DTPA2F is 217 °C (the first upward scan, Fig. 1a) and the glass transition temperature (T_g) is 83 °C (the second upward scan, Fig. 1a). Considering that a T_g/T_m value of approximately 2/3 is the lower bound threshold for good glass

formation, the high T_g/T_m value of 356.15 K/490.15 K ≈ 0.73 for DTPA2F suggests that it is likely to form stable glassy materials.[44] Fortunately, we can successfully fabricate DTPA2F glass with a size of 24 cm^2 (Fig. S15a†) through a simple melt quenching method.[19] In comparison, TPABTPA also exhibited excellent thermal stability (T_d = 432 °C, Fig. S16a†), but its DSC curve revealed only a melting point (T_m = 241 °C, Fig. S16b†), indicating it cannot form stable glassy materials.[45] These results suggest that the introduction of F atoms lowered the melting point of the DTPA2F molecule and facilitated the appearance of a glass transition temperature, enabling the preparation of a glassy material.

Based on the prepared DTPA2F glass films, we conducted a comprehensive analysis of their transparency and scintillation performance. As shown in Fig. 3b, the material is colorless and transparent under natural light, with a transmittance exceeding 87% in the range of 450–800 nm. And under 365 nm UV light, it emits bright blue luminescence. Its high transparency, achieved by reducing light scattering, enhances light output efficiency, making it more appealing for optical applications.[46] Besides, as shown in Fig. S17 and S18,† the Fourier-transform infrared (FTIR) and Raman spectra of the DTPA2F molecule in both powder and glass states are essentially identical, indicating that the transition from powder to glass did not alter the molecular structure and bonding.[14] According to the steady-state PL

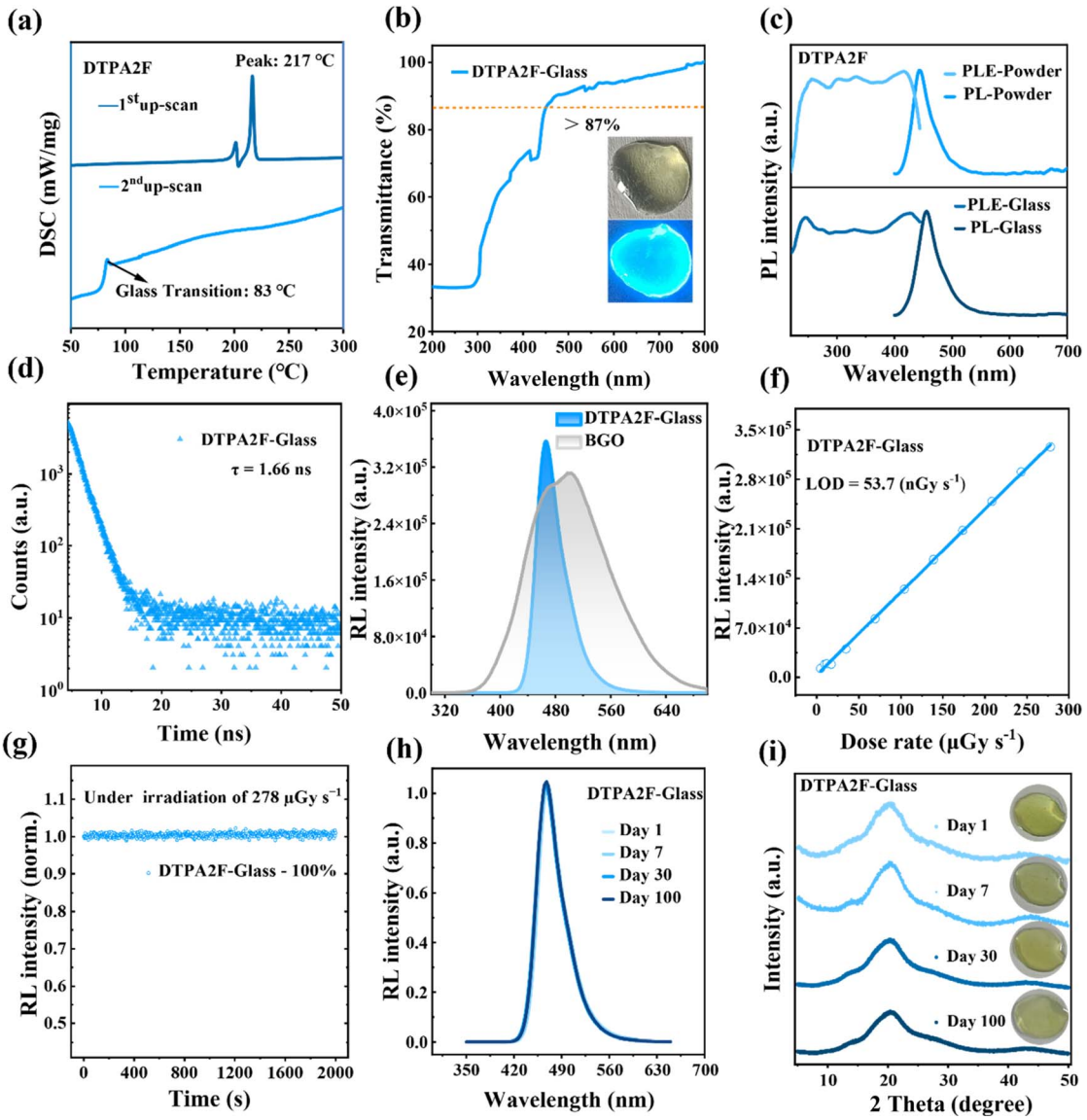

Fig. 3 Thermal and scintillation properties of DTPA2F glassy materials. (a) DSC curves of DTPA2F. (b) The ultraviolet-visible transmittance spectrum of DTPA2F glass, with inset images showing DTPA2F glass under visible and UV light. (c) The excitation and emission spectra of DTPA2F powder and DTPA2F-Glass. (d) Time-resolved PL decay spectra of DTPA2F-Glass. (e) RL spectra of BGO and DTPA2F-Glass under an X-ray dose rate of 278 μGy s^{-1}. (f) The linear response of RL intensity to various X-ray dose rates for DTPA2F-Glass. (g) Stability of DTPA2F-Glass under continuous irradiation for 2000 s (278 μGy s^{-1}). Changes in (h) RL intensity, and (i) corresponding PXRD patterns and morphological images of DTPA2F glass after 100 days of storage under ambient conditions.

spectra, the emission peaks of the glassy and powder samples are at 443 and 453 nm, respectively (Fig. 3c). The slight red shift of 10 nm in the glass state may be due to the higher disorder in the glass material, which can affect the energy of electronic transitions.[47] However, their PL excitation (PLE) spectra have nearly identical profiles (Fig. 3c), indicating that the emission from both the glassy and crystalline samples originates from the relaxation of the same excited state.[14]

Then we tested and analyzed the scintillation performance of DTPA2F glass. As shown in Fig. 3d, the RL intensity of DTPA2F glass is 3.57×10^5 a.u., which is 77.1% and 114% that of the DTPA2F powder and BGO single crystal, respectively. Further measurements of the X-ray-excited luminescence spectra allowed us to calculate its LOD which was as low as 53.7 nGy s^{-1} (Fig. S13c† and 3e).[36] Moreover, using BGO as a reference, we calculated that the relative light yield of DTPA2F glass could reach 28 341 ± 246 photons MeV^{-1}, which exceeds that of most reported metal halide glassy scintillator materials (Table S5†). The excellent scintillation performance of DTPA2F glass primarily stems from its high PLQY in the amorphous state. Further measurements revealed that the Φ_f of DTPA2F glass remains as high as 49.8%, which is 73.5% that of its crystalline powder. This indicates that the PLQY attenuation rate of DTPA2F from crystalline to amorphous glass state is only 26.5%, which is significantly lower than that of all reported metal halide materials (Table S5†).[48] Additionally, the decay time of DTPA2F glass is 1.66 ns (Fig. 3d), maintaining the characteristic short decay lifetime of hot exciton dyes, and this value is more than three orders of magnitude lower than that of reported metal halide glass scintillators (Table S5†).[9] Therefore, compared to the reported metal halide glass scintillators, DTPA2F glass offers a combination of higher relative light yield, excellent optical transmittance, and the fastest decay time, making it an amorphous scintillator material with outstanding overall performance.

Overall, glass is an amorphous intermediate state material, and stability is a vital metric for assessing glassy materials. We evaluated the stability of the glass state under a continuous X-ray dose of 278 μGy s^{-1} for 2000 s, maintaining nearly 100% of its initial radioluminescence intensity (Fig. 3g). In order to better verify its irradiation stability, it was made to undergo four days of periodic X-ray exposure (30 min per day, 64 cycles in total), after which the radioluminescence intensity still remained above 99% of the initial value (Fig. S19†). Further, XRD analysis before and after irradiation confirmed the structural integrity (Fig. S20†), demonstrating excellent irradiation

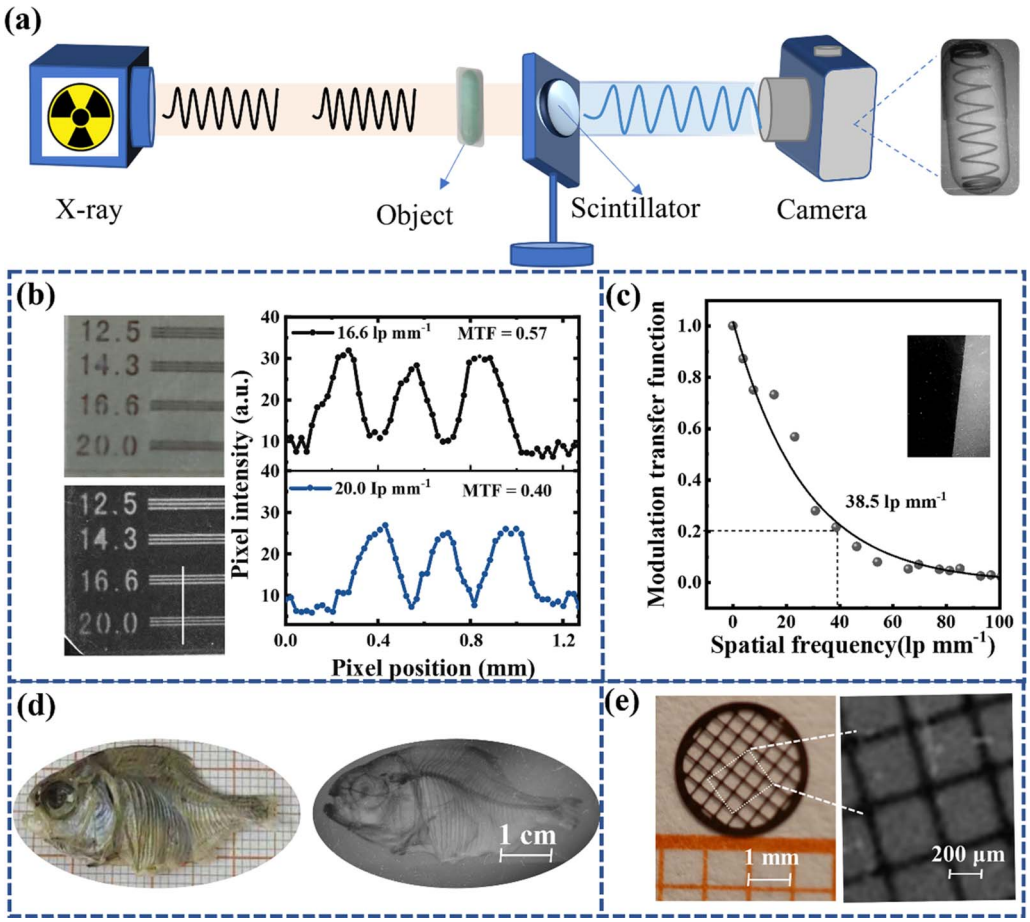

Fig. 4 High-resolution X-ray imaging using the DTPA2F glassy screen. (a) Schematic diagram of the X-ray imaging system. (b) X-ray exposure contrast image of line-pair card, with the corresponding plot of pixel intensity *versus* pixel positions along the white line. (c) MTF *versus* spatial frequency, derived from edge image analysis. Samples imaged under X-ray and visible light: (d) a dried fish and (e) a copper mesh.

stability and expanding the feasible applications of this glassy-state material. Additional studies on environmental stability were conducted by exposing the glassy-state scintillator material to air. As shown in Fig. 3h, after placing the DTPA2F glass in air for 100 days, its RL intensity showed no signs of decay. The XRD tests conducted before and after this period also yielded consistent results, indicating that the prepared glassy-state scintillator possesses good environmental stability (Fig. 3i). Additionally, the DTPA2F glass maintained high transparency, with no signs of powder precipitation observed. This balance of transparency, luminous lifetime, radioluminescence intensity, and stability greatly enhances the application of organic scintillators in high-resolution imaging. At the same time, the crystallization resistance of the glass film was evaluated by heating it to 60, 80, and 100 °C, respectively. When the heating temperature was below 80 °C, the material remained transparent with no signs of crystallization. However, at 100 °C, noticeable crystallization occurred. As shown in Fig. S21,† XRD testing confirmed that the samples maintained an amorphous state when the temperature did not exceed 80 °C, indicating its excellent thermal stability. This balance between transparency, luminous lifetime, radioluminescence intensity, and stability greatly benefits the application of organic scintillators in high-resolution imaging.

To evaluate the X-ray imaging capability of DTPA2F glass films, we constructed an X-ray imaging system, as shown in Fig. 4a. Notably, the DTPA2F glass scintillator screen, fabricated *via* the melt-quenching method, exhibited remarkable flatness, even under scanning electron microscope (SEM) magnification up to 100 times (Fig. S15b†). In addition, the sample remains highly smooth even after more than 100 days of placement (Fig. S15c†). This high level of flatness is advantageous for minimizing optical crosstalk during imaging, thereby enhancing image clarity. Further X-ray imaging tests using a line pair card demonstrated the visibility of 20 lp mm^{-1} gaps, as depicted in Fig. 4b. Using ImageJ software, we generated a curve of pixel intensity *versus* pixel position, and the modulation transfer function (MTF) values at 16.6 lp mm^{-1} and 20 lp mm^{-1} are calculated to be 0.57 and 0.40, respectively,[40] indicating the excellent spatial resolution of DTPA2F glass film. To further assess its imaging capabilities, we employed the slanted-edge method[5] for detailed imaging and analysis of the prepared glass films (Fig. 4c). The results showed an X-ray imaging resolution of 38.5 lp mm^{-1} @ MTF = 0.2, surpassing most reported organic scintillators (Table S6†). The X-ray images captured using the scintillator screen clearly depicted the internal bone structure of a fish approximately 6 cm in length, as well as distinct vertical lines in a copper mesh. Moreover, we also prepared powdered scintillator films using a filtration method[49] and evaluated their X-ray imaging capabilities with the same line pair card, small fish, and spring (Fig. S22†). As shown in Fig. S23,† the spatial resolution of filtered films made from DTPA2F powder is 14.3 lp mm^{-1} @ MTF = 0.228, which is significantly lower than that of the DTPA2F glass films. This result further confirms the superior spatial resolution imaging capability of DTPA2F glass films and underscores the effectiveness of fabricating organic glass films to enhance light output efficiency and achieve high-resolution imaging.

Conclusions

In summary, we present a novel hot exciton organic glassy scintillator for the first time, featuring a mechanism of hybrid localized and charge transfer excited states, capable of efficiently utilizing both singlet and triplet excitons to achieve rapid and highly efficient scintillation. The obtained DTPA2F glass scintillator demonstrates remarkable optical properties, including a transmittance of over 87% @ 450–800 nm, a PLQY of up to 49.8%, and a relative light yield of 28 341 ± 246 photons MeV^{-1}. Additionally, it exhibits an ultrafast decay time of 1.66 ns and a low detection limit of 53.7 nGy s^{-1}, which is only 1/102nd of the dose rate compared to commercial X-ray diagnostics. Notably, DTPA2F glass shows excellent radiation resistance and superior environmental stability, with no recrystallization or degradation observed after more than 100 days under ambient conditions. Leveraging its high transmittance, fast scintillation time and high RL intensity, we prepared a glassy scintillator screen with an area of up to 24 cm^2 using a simple melt quenching method, achieving a spatial resolution of up to 38.5 lp mm^{-1} in X-ray imaging. This work underscores the potential of hot exciton organic glass scintillators for developing large-area, highly transparent, efficient, and fast scintillators, offering a promising pathway for future advancements in scintillator technology.

Data availability

The data supporting this study's findings are available from the corresponding author upon reasonable request.

Author contributions

X. Yang completed the experiments and wrote the manuscript, J.-R. Chen assisted in the imaging measurements, and Y. Zhang helped with the theoretical calculations. Y.-M. Di helped with the Crystal modification and G.-Z. Zhang helped with the optical physics test. M.-J. Lin, S.-H Chen and H.-M. Chen supervised and revised the manuscript. All authors discussed the results and commented on the manuscript.

Conflicts of interest

There are no conflicts to declare.

Acknowledgements

This work was supported by the National Natural Science Foundation of China (22201042, 22371047), Natural Science Foundation of Fujian Province (2022J05118, 2024J01156), Collaborative Innovation Platform Project of Fu-Xia-Quan National Independent Innovation Demonstration Zone (2022-P-021) and Fujian Province Science and Technology (2022H4022).

Notes and references

1 K. M. McCall, K. Sakhatskyi, E. Lehmann, B. Walfort, A. S. Losko, F. Montanarella, M. I. Bodnarchuk, F. Krieg, Y. Kelestemur, D. Mannes, Y. Shynkarenko, S. Yakunin and M. V. Kovalenko, Fast Neutron Imaging with Semiconductor Nanocrystal Scintillators, *ACS Nano*, 2020, **14**, 14686–14697.

2 M. Chen, L. Sun, X. Ou, H. Yang, X. Liu, H. Dong, W. Hu and X. Duan, Organic Semiconductor Single Crystals for X-ray Imaging, *Adv. Mater.*, 2021, **33**, 2104749.

3 G. Zhang, F. Chen, Y. Di, S. Yuan, Y. Zhang, X. Quan, Y. Chen, H. Chen and M. Lin, Guest-Induced Thermally Activated Delayed Fluorescence Organic Supramolcular Macrocycle Scintillators for High-Resolution X-Ray Imaging, *Adv. Funct. Mater.*, 2024, **34**, 2404123.

4 N. Gan, X. Zou, M. Dong, Y. Wang, X. Wang, A. Lv, Z. Song, Y. Zhang, W. Gong, Z. Zhao, Z. Wang, Z. Zhou, H. Ma, X. Liu, Q. Chen, H. Shi, H. Yang, L. Gu, Z. An and W. Huang, Organic phosphorescent scintillation from copolymers by X-ray irradiation, *Nat. Commun.*, 2022, **13**, 3995.

5 S. Yuan, G. Zhang, F. Chen, J. Chen, Y. Zhang, Y. Di, Y. Chen, Y. Zhu, M. Lin and H. Chen, Thermally Activated Delayed Fluorescent Ag(I) Complexes for Highly Efficient Scintillation and High-Resolution X-Ray Imaging, *Adv. Funct. Mater.*, 2024, **34**, 2400436.

6 Y. Huo, J. Lv, M. Wang, Z. Duan, H. Qi, S. Wang, Y. Liu, L. Peng, S. Ying and S. Yan, Simple excited-state modification toward a deep-blue hybridized local and charge-transfer (HLCT) fluorophore and non-doped organic light-emitting diodes, *J. Mater. Chem. C*, 2023, **11**, 6347–6353.

7 W. Li, Y. Pan, R. Xiao, Q. Peng, S. Zhang, D. Ma, F. Li, F. Shen, Y. Wang, B. Yang and Y. Ma, Employing ~100% Excitons in OLEDs by Utilizing a Fluorescent Molecule with Hybridized Local and Charge-Transfer Excited State, *Adv. Funct. Mater.*, 2014, **24**, 1609–1614.

8 Y. Zhang, M. Chen, X. Wang, M. Lin, H. Wang, W. Li, F. Chen, Q. Liao, H. Chen, Q. Chen, M. Lin and H. Yang, Efficient and Fast X-Ray Luminescence in Organic Phosphors Through High-Level Triplet-Singlet Reverse Intersystem Crossing, *CCS Chem.*, 2024, **6**, 334–341.

9 X. Du, S. Zhao, L. Wang, H. Wu, F. Ye, K.-H. Xue, S. Peng, J. Xia, Z. Sang, D. Zhang, Z. Xiong, Z. Zheng, L. Xu, G. Niu and J. Tang, Efficient and ultrafast organic scintillators by hot exciton manipulation, *Nat. Photonics*, 2024, **18**, 162–169.

10 A. Yoneyama, R. Baba and M. Kawamoto, Quantitative analysis of the physical properties of CsI, GAGG, LuAG, CWO, YAG, BGO, and GOS scintillators using 10-, 20- and 34-keV monochromated synchrotron radiation, *Opt. Mater.*, 2021, **11**, 398–411.

11 Y. W. Heinson, A. Chakrabarti and C. M. Sorensen, A light-scattering study of Al2O3 abrasives of various grit sizes, *J. Quant. Spectrosc. Radiat. Transf.*, 2016, **180**, 84–91.

12 J. Ma, W. Zhu, L. Lei, D. Deng, Y. Hua, Y. M. Yang, S. Xu and P. N. Prasad, Highly Efficient NaGdF4:Ce/Tb Nanoscintillator with Reduced Afterglow and Light Scattering for High-Resolution X-ray Imaging, *ACS Appl. Mater. Interfaces*, 2021, **13**, 44596–44603.

13 L. Li, J. Chen, Z. Wen, J. Guo, Q. Wang and H. Guo, X-ray imaging scintillator: Tb3+-doped oxyfluoride aluminosilicate glass, *Ceram. Int.*, 2024, **50**, 757–763.

14 J. B. Luo, J. H. Wei, Z. Z. Zhang, Z. L. He and D. B. Kuang, A Melt-Quenched Luminescent Glass of an Organic-Inorganic Manganese Halide as a Large-Area Scintillator for Radiation Detection, *Angew. Chem., Int. Ed.*, 2023, **62**, e202216504.

15 Z. Xu, N. Li, X. Yan, X. Wang, T. He, Z. Yang and S. Liu, Transparent 0D Antimony Halides Glassy Wafer with Near-Unity Photoluminescence Quantum Yield for High Spatial Resolution X-Ray Imaging, *Adv. Opt. Mater.*, 2024, **12**, 2301477.

16 B. Li, J. Jin, M. Yin, K. Han, Y. Zhang, X. Zhang, A. Zhang, Z. Xia and Y. Xu, In situ recrystallization of zero-dimensional hybrid metal halide glass-ceramics toward improved scintillation performance, *Chem. Sci.*, 2023, **14**, 12238–12245.

17 B. Li, J. Jin, X. Liu, M. Yin, X. Zhang, Z. Xia and Y. Xu, Multiphase Transformation in Hybrid Copper(I)-Based Halides Enable Improved X-ray Scintillation and Real-Time Imaging, *ACS Mater. Lett.*, 2024, **6**, 1542–1548.

18 X. Wang, X. Zhang, Y. Liu and Y. Zhang, Shape-on-demand synthesis of luminescent (ETP)2MnBr4 glass scintillator, *Chem. Eng. J.*, 2024, **483**, 149239.

19 X. Quan, G. Z. Zhang, Y. Zhang, Q. Liao, H. M. Chen and M. J. Lin, Low-Cost, Large-Area, and Highly Transparent Organic Glassy Scintillators for High Resolution X-Ray Imaging, *Adv. Opt. Mater.*, 2024, **12**, 2400113.

20 S. K. Jeon, S. K. Shin, J. Y. Lee, Y. Han, H.-S. Choi, C. W. Han and H. C. Choi, Key factors of exciplex emission: Exciton binding and intermolecular molecular orbital overlap, *Org. Electron.*, 2018, **63**, 283–288.

21 J. Chen, H. Liu, J. Guo, J. Wang, N. Qiu, S. Xiao, J. Chi, D. Yang, D. Ma, Z. Zhao and B. Z. Tang, Robust Luminescent Molecules with High-Level Reverse Intersystem Crossing for Efficient Near Ultraviolet Organic Light-Emitting Diodes, *Angew. Chem., Int. Ed.*, 2022, **61**, e202116810.

22 G. Li, K. Xu, J. Zheng, X. Fang, W. Lou, F. Zhan, C. Deng, Y.-F. Yang, Q. Zhang and Y. She, High-Performance Ultraviolet Organic Light-Emitting Diodes Enabled by Double Boron–Oxygen-Embedded Benzo[m]tetraphene Emitters, *J. Am. Chem. Soc.*, 2024, **146**, 1667–1680.

23 J. Li, M. Zhang, T. Li, D. Guo, T. Tian and H. Zhang, Realization of switching between TADF and HLCT emissions through modulation of the intramolecular charge transfer character, *J. Mater. Chem. C*, 2022, **10**, 13124–13136.

24 W. Wang, J. Bian, K. Chen, C. Li, Y. Long, H. Huang, L. Jiang, J. Zhao, S. Liu, Z. Chi, J. Xu and Y. Zhang, Achieving Record External Quantum Efficiency of 11.5% in Solution-Processable Deep-Blue Organic Light-Emitting Diodes Utilizing Hot Exciton Mechanism, *Angew. Chem., Int. Ed.*, 2024, **63**, e202318782.

25 H. Sun, J. Jin, H. Ren, B. Liu, Q. Wu, Y. Mei, J. Wang, J. Yang, D. Liu and J. Li, Fine tuning of excited states by trifluoromethylphenyl for blue-shifted color and enhanced EQEs in thermally activated delayed fluorescence emitters, *Dyes Pigments*, 2024, **228**, 112233.

26 C. Liao, B. Chen, Q. Xie, X. Li, H. Liu and S. Wang, A Breakthrough in Solution-Processed Ultra-Deep-Blue HLCT OLEDs: A Record External Quantum Efficiency Exceeding 10% Based on Novel V-Shaped Emitters, *Adv. Mater.*, 2023, **35**, 2305310.

27 H. Zhang, G. Li, X. Guo, K. Zhang, B. Zhang, X. Guo, Y. Li, J. Fan, Z. Wang, D. Ma and B. Z. Tang, High-Performance Ultraviolet Organic Light-Emitting Diode Enabled by High-Lying Reverse Intersystem Crossing, *Angew. Chem., Int. Ed.*, 2021, **60**, 22241–22247.

28 W. Mo, Z. Zhu, F. Kong, X. Li, Y. Chen, H. Liu, Z. Cheng, H. Ma and B. Li, Controllable synthesis of conjugated microporous polymer films for ultrasensitive detection of chemical warfare agents, *Nat. Commun.*, 2022, **13**, 5189.

29 Y. Shao, H. Cai, F. Zhao, Z. Song and Q. Liu, Efficient Blue-Violet Phosphor with Small Stokes-Shift for Full-Spectrum Lighting, *Laser Photon. Rev.*, 2023, **17**, 2300342.

30 B. Guzelturk, B. T. Diroll, J. P. Cassidy, D. Harankahage, M. Hua, X.-M. Lin, V. Iyer, R. D. Schaller, B. J. Lawrie and M. Zamkov, Bright and durable scintillation from colloidal quantum shells, *Nat. Commun.*, 2024, **15**, 4274.

31 M. Fang, J. Yang and Z. Li, Light emission of organic luminogens: Generation, mechanism and application, *Prog. Mater. Sci.*, 2022, **125**, 100914.

32 A. V. Parwani, Expression of Glypican 3 in Ovarian and Extragonadal Germ Cell Tumors, *Yearbook of Pathology and Laboratory Medicine*, 2009, vol. 11, pp. 19–32.

33 C. Wang, W. Chi, Q. Qiao, D. Tan, Z. Xu and X. Liu, Twisted intramolecular charge transfer (TICT) and twists beyond TICT: from mechanisms to rational designs of bright and sensitive fluorophores, *Chem. Soc. Rev.*, 2021, **50**, 12656–12678.

34 W. Ma, Y. Su, Q. Zhang, C. Deng, L. Pasquali, W. Zhu, Y. Tian, P. Ran, Z. Chen, G. Yang, G. Liang, T. Liu, H. Zhu, P. Huang, H. Zhong, K. Wang, S. Peng, J. Xia, H. Liu, X. Liu and Y. M. Yang, Thermally activated delayed fluorescence (TADF) organic molecules for efficient X-ray scintillation and imaging, *Nat. Mater.*, 2022, **21**, 210–216.

35 J.-X. Wang, L. Gutiérrez-Arzaluz, X. Wang, T. He, Y. Zhang, M. Eddaoudi, O. M. Bakr and O. F. Mohammed, Heavy-atom engineering of thermally activated delayed fluorophores for high-performance X-ray imaging scintillators, *Nat. Photonics*, 2022, **16**, 869–875.

36 H. Chen, M. Lin, Y. Zhu, D. Zhang, J. Chen, Q. Wei, S. Yuan, Y. Liao, F. Chen, Y. Chen, M. Lin and X. Fang, Halogen-bonding boosting the high performance X-ray imaging of organic scintillators, *Small*, 2024, **20**, 2307277.

37 X. Wang, G. Niu, Z. Zhou, Z. Song, K. Qin, X. Yao, Z. Yang, X. Wang, H. Wang, Z. Liu, C. Yin, H. Ma, K. Shen, H. Shi, J. Yin, Q. Chen, Z. An and W. Huang, Halogenated Thermally Activated Delayed Fluorescence Materials for Efficient Scintillation, *Research*, 2023, **6**, 0090.

38 W. Li, Y. Li, Y. Wang, Z. Zhou, C. Wang, Y. Sun, J. Sheng, J. Xiao, Q. Wang, S. Kurosawa, M. Buryi, D. John, K. Paurová, M. Nikl, X. OuYang and Y. Wu, Highly Efficient and Flexible Scintillation Screen Based on Organic Mn(II) Halide Hybrids toward Planar and Nonplanar X-Ray Imaging, *Laser Photon. Rev.*, 2024, **18**, 2300860.

39 X. Wang, H. Shi, H. Ma, W. Ye, L. Song, J. Zan, X. Yao, X. Ou, G. Yang, Z. Zhao, M. Singh, C. Lin, H. Wang, W. Jia, Q. Wang, J. Zhi, C. Dong, X. Jiang, Y. Tang, X. Xie, Y. Yang, J. Wang, Q. Chen, Y. Wang, H. Yang, G. Zhang, Z. An, X. Liu and W. Huang, Organic phosphors with bright triplet excitons for efficient X-ray-excited luminescence, *Nat. Photonics*, 2021, **15**, 187–192.

40 H. Chen, M. Lin, C. Zhao, D. Zhang, Y. Zhang, F. Chen, Y. Chen, X. Fang, Q. Liao, H. Meng and M. Lin, Highly Efficient, Low-Dose, and Ultrafast Carbazole X-Ray Scintillators, *Adv. Opt. Mater.*, 2023, **11**, 2300365.

41 M. Lang, C. L. Tracy, R. I. Palomares, F. Zhang, D. Severin, M. Bender, C. Trautmann, C. Park, V. B. Prakapenka, V. A. Skuratov and R. C. Ewing, Characterization of ion-induced radiation effects in nuclear materials using synchrotron x-ray techniques, *J. Mater. Res.*, 2015, **30**, 1366–1379.

42 A. Jana, S. Park, S. Cho, H. Kim and H. Im, Bounce back with triplet excitons for efficient X-ray scintillation, *Matter*, 2022, **5**, 20–22.

43 D. J. Daniel, P. Karuppasamy, P. Q. Vuong and H. J. Kim, Synthesis, crystal growth, structural and physicochemical properties of an organic single crystal (C11H16N2O4) for fast scintillation and NLO applications, *CrystEngComm*, 2022, **24**, 2867–2877.

44 K. Koperwas, K. Adrjanowicz, Z. Wojnarowska, A. Jedrzejowska, J. Knapik and M. Paluch, Glass-Forming Tendency of Molecular Liquids and the Strength of the Intermolecular Attractions, *Sci. Rep.*, 2016, **6**, 36934.

45 A. L. Greer, New horizons for glass formation and stability, *Nat. Mater.*, 2015, **14**, 542–546.

46 M. A. Ali, W. M. W. Winters, M. A. Mohamed, D. Tan, G. Zheng, R. S. K. Madsen, O. V. Magdysyuk, M. Diaz-Lopez, B. Cai, N. Gong, Y. Xu, I. Hung, Z. Gan, S. Sen, H. T. Sun, T. D. Bennett, X. Liu, Y. Yue and J. Qiu, Fabrication of Super-Sized Metal Inorganic-Organic Hybrid Glass with Supramolecular Network *via* Crystallization-Suppressing Approach, *Angew. Chem., Int. Ed.*, 2023, **62**, e202218094.

47 H. Zhang, Z. Zhao, A. T. Turley, L. Wang, P. R. McGonigal, Y. Tu, Y. Li, Z. Wang, R. T. K. Kwok, J. W. Y. Lam and B. Z. Tang, Aggregate Science: From Structures to Properties, *Adv. Mater.*, 2020, **32**, 2001457.

48 T. Feng, Z. a. Zhou, Y. n. An, L. Chen, Y. Fu, S. Zhou, N. Wang, J. Zheng and C. Sun, Large-Area Transparent Antimony-Based Perovskite Glass for High-Resolution X-ray Imaging, *ACS Nano*, 2024, **18**, 16715–16725.

49 Y.-H. Chen, G.-Z. Zhang, F.-H. Chen, S.-Q. Zhang, X. Fang, H.-M. Chen and M.-J. Lin, Halogen-bonded charge-transfer co-crystal scintillators for high-resolution X-ray imaging, *Chem. Sci.*, 2024, **15**, 7659–7666.